JACS
JOURNAL OF THE AMERICAN CHEMICAL SOCIETY

Article

pubs.acs.org/JACS

Substituent Effects on the pH Sensitivity of Acetals and Ketals and Their Correlation with Encapsulation Stability in Polymeric Nanogels

Bin Liu[†] and S. Thayumanavan*[,†,‡]

[†]Department of Chemistry, [‡]Center for Bioactive Delivery, Institute for Applied Life Sciences, University of Massachusetts, Amherst, Massachusetts 01003, United States

Supporting Information

ABSTRACT: The effect of structural variations in acetal- and ketal-based linkers upon their degradation kinetics is studied through the design, synthesis, and study of six series of molecules, comprising a total of 18 different molecules. Through this systematic study, we show that the structural fine-tuning of the linkers allows access to variations in kinetics of degradation of more than 6 orders of magnitude. Hammett correlations show that the ρ value for the hydrolysis of benzylidene acetals is about −4.06, which is comparable to an S_N1-like process. This shows that there is a strong, developing positive charge at the benzylic position in the transition state during the degradation of acetals. This positively charged transition state is consistent with the relative degradation rates of acetals vs ketals (correlated to stabilities of 1°, 2°, and 3° carboxonium ion type intermediates) and the observed effect of proximal electron-withdrawing groups upon the degradation rates. Following this, we studied whether the degradation kinetics study correlates with pH-sensitive variations in the host−guest characteristics of polymeric nanogels that contains these acetal or ketal moieties as cross-linking functionalities. Indeed, the trends observed in the small molecule degradation have clear correlations with the encapsulation stability of guest molecules within these polymeric nanogels. The implications of this fundamental study extend to a broad range of applications, well beyond the polymeric nanogel examples studied here.

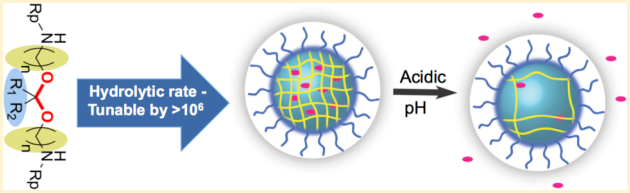

INTRODUCTION

Materials that predictably respond to a specific environment change through changes in their physicochemical properties have attracted attention due to potential applications in areas ranging from material science to biomedicine.[1−3] The environmental change, i.e., the input signal, in these cases can be physical (e.g., temperature, light, ultrasonic, magnetic, and electrical), chemical (e.g., pH, redox, and ionic), or biological (e.g., protein, carbohydrates, and nucleic acids) in nature. Among this diverse range of inputs that are pursued, pH has attracted significant attention mainly because of its simplicity and its biological relevance. pH is simple in that the diffusion of protons inside nanomaterials is a relatively facile process, because of its small size. pH is also very relevant in human biology, as specific pH variations have been identified from subcellular levels to tissue levels.[4] For example, the pH of the typical extracellular environment is about 7.4, which decreases to ∼5.5−6.5 inside the endosome and further to 4.5−5.5 inside the lysosome.[4−7] Also, although the pH is ∼7.4 in the extracellular environment of normal tissues, it has been shown that the pH around certain tumor tissues is ∼6.5 due to the hypoxia-induced production of excess lactic acid in the tumor microenvironments.[8−11] Thus, pH responsive materials have been explored for many biological applications, including sensing, diagnostics, tissue engineering, and targeted drug delivery.[12−14]

pH responsive materials can be broadly classified into two main categories in which: (i) the responsive units are based on noncleavable, ionizable functional groups where pH-induced charge variations play a key role (e.g., amines and carboxylic acids);[12,15] (ii) the key functionalities are based on chemical linkages that degrade due to pH variations (e.g., acetal, ketal, imine, hydrazine, *cis*-aconityl, and β-thiol ester).[15−18] Cleavable linkers have been widely used as building blocks for polymers, nanoparticles, and antibody-drug conjugates, as well as in protein purification and solid phase synthesis.[19−21]

Among pH-sensitive linkers, acetals and ketals have attracted significant attention, because they yield charge-neutral and potentially nontoxic by products upon cleavage. The mechanism of the hydrolysis of the acetals and ketals has been a subject of interest since the 1960s.[22−24] More recently, these substituted methylene glycol diether materials have been pursued in a variety of areas including controlled release applications,[25−27] nucleic acid delivery,[28] degradable polymers,[29−33] temporary masking agents for polymers and nanoassemblies,[26,34−36] and pro-drug formulations.[37−39] Despite such widespread use, there is no report that provides a systematic understanding on the structural factors that affect the pH sensitivity of these functionalities. An understanding of the dynamic range, which each functional group variation can

Received: October 26, 2016
Published: January 20, 2017

DOI: 10.1021/jacs.6b11181
J. Am. Chem. Soc. 2017, 139, 2306−2317

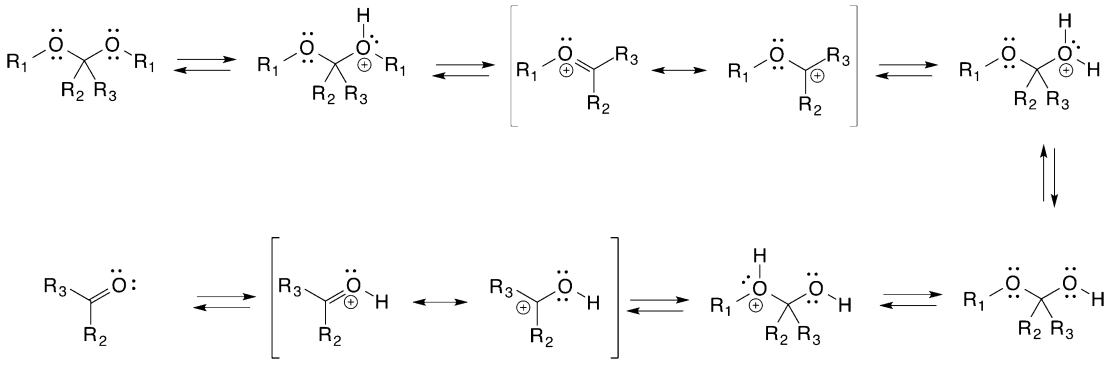

Figure 1. Well-established mechanism of the hydrolysis of acetals and ketals. Formation of the resonance-stabilized caboxonium ion intermediate, shown within the square bracket in the top, is considered to be the rate-determining step of this cleavage reaction. Therefore, structures of R_1, R_2, and R_3 will all influence the kinetics of this cleavage reaction.

provide, will fundamentally impact the utility of these functionalities in designing biomaterials, as these will provide a robust and convenient framework for choosing the appropriate linker for a specific application. This is important because the variations in pH in different locations are rather subtle and the drug release profile requirements are quite different in various applications. In drug delivery applications for example, extended release of drugs is required for the treatment of chronic diseases,[40,41] whereas a targeted and burst release is needed for diseases such as cancer and certain acute inflammatory diseases.[42,43] On the other hand, in applications such as protein purification, it is critical that the cleavage is achieved under mild reaction conditions in order to prevent possible denaturation. In this paper, several series of acetals and ketals linker have been designed and studied for their relative pH sensitivity. As a first step to test the fidelity of such a study in drug delivery applications, we incorporate these moieties within polymeric nanoparticles using our previous emulsion-free method[44,45] and evaluate their pH-induced variations in encapsulation stability of guest molecules.

RESULTS AND DISCUSSION

Acetals and ketals are known to be quite stable under basic conditions, but readily hydrolyze to the corresponding carbonyl compound (aldehyde and ketone) and alcohol under acidic conditions. To establish the design variations needed for this study, we first considered the mechanism of acid-catalyzed cleavage of these diethers (Figure 1). In the hydrolysis process, formation of the resonance-stabilized carboxonium ion intermediate has been suggested to be the rate-determining step.[22] Therefore, the stability of this carboxonium ion would dictate the hydrolysis rate of the corresponding acetal or ketal; i.e., if the intermediate carboxonium ion is more stabilized, then the hydrolysis rate would be faster. Because of the cationic character of the intermediate, electron-donating group substituents are generally expected to stabilize the intermediate and thus accelerate hydrolysis. Also, in general, the R_1 group is likely to have greater contributions based on inductive effects, whereas R_2 and R_3 could have contributions from inductive and resonance effects. Thus, a series of 18 different ketal or acetal based molecules, with different R_1, R_2 and R_3 groups, were designed and synthesized. Structures of these molecules are shown in Figure 2.

Note that a key objective of this work is to compare the small molecule sensitivity with the corresponding functional groups being used as cross-linkers in polymeric nanoparticles. Because the cross-links in these nanoparticles will be based on amide moieties, the small molecules studied here are also based on the corresponding amides. These molecules are divided into six different series, where each of the series probes a specific structural correlation within these acetal or ketal based cross-linkers, as shown in Figure 2. Syntheses of these molecules are detailed in the Supporting Information.

Although the hydrolytic stabilities of these molecules are ideally studied in aqueous solutions, many of these targeted molecules proved to be insoluble. To exclude variations in extraneous factors such as hydrophobicity induced aggregation or solution heterogeneity, a homogeneous solution system was chosen to monitor the intrinsic hydrolysis kinetics. In general, a mixture of 0.3 mL CD_3CN and 0.1 mL PB buffer in D_2O was used as the solvent, where the concentration of the molecules under investigation was kept at 25 mM at pH 5. The hydrolysis kinetics was assessed by monitoring the NMR of the solution at different time intervals at 25 °C. The typical process and the data are exemplified using the ketal molecule **3**, as shown in Figure 3. Key changes in the evolution of the ^{1}H NMR spectrum involve the gradual decrease in the peak at 1.29 ppm, with the concurrent increase in the intensity of the peak at 2.09 ppm. The peak at 1.29 ppm is attributed to the methyl group connected to ketal moiety, whereas the peak at 2.09 ppm represents the formation of the acetone product. Percentage degradation of the ketal moiety was thus calculated either by the NMR signals from the rate of disappearance of the ketal (or acetal) substrate moieties or from the rate of appearance of the ketone (or aldehyde) product functional groups. The reactions obeyed first-order reaction kinetics and hydrolysis rates were obtained through an exponential fit with excellent correlation functions (typical $R^2 > 0.99$). To quantify the relative rates of hydrolysis, half-life of these pH-sensitive functional groups were extracted from these plots. In such a case, all the experiments were performed three times and the error values of $t_{1/2}$ represent the standard deviation from these three trials. The half-life of **3** under these conditions was found to be 32.33 ± 0.90 h. Further, the effect of pH on the hydrolysis kinetics was performed, and the results are shown in Figure 4. The hydrolysis kinetics dramatically decreased with increasing pH. For instance, the hydrolysis rate decreased by ~3 times, upon changing the pH from 5.0 to 5.5, and by another 3 times at pH = 6.0. When the pH was increased to 6.5, the hydrolysis rate was decreased another 6 times. This molecule was quite stable and exhibited no measurable hydrolysis under pH = 7.4 for 7 days.

DOI: 10.1021/jacs.6b11181
J. Am. Chem. Soc. 2017, 139, 2306−2317

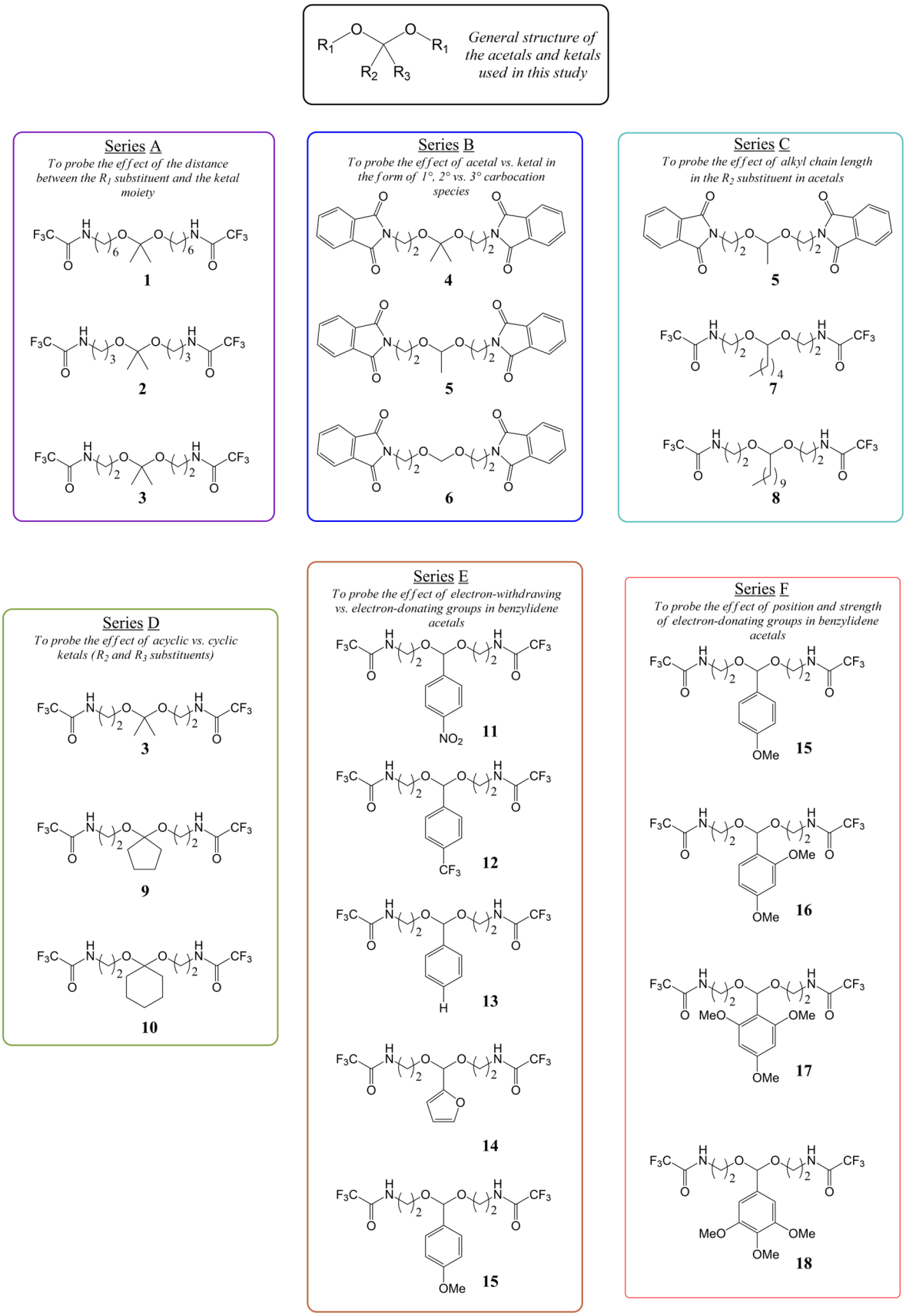

Figure 2. Structures of the acetal and ketal small molecules studies in this work.

In the first series of molecules, we vary the distance between the amide functional group and the ketal moiety (Series A in Figure 2). The amide moiety is an inductively electron-withdrawing moiety and thus this series interrogates the effect

DOI: 10.1021/jacs.6b11181
J. Am. Chem. Soc. 2017, 139, 2306−2317

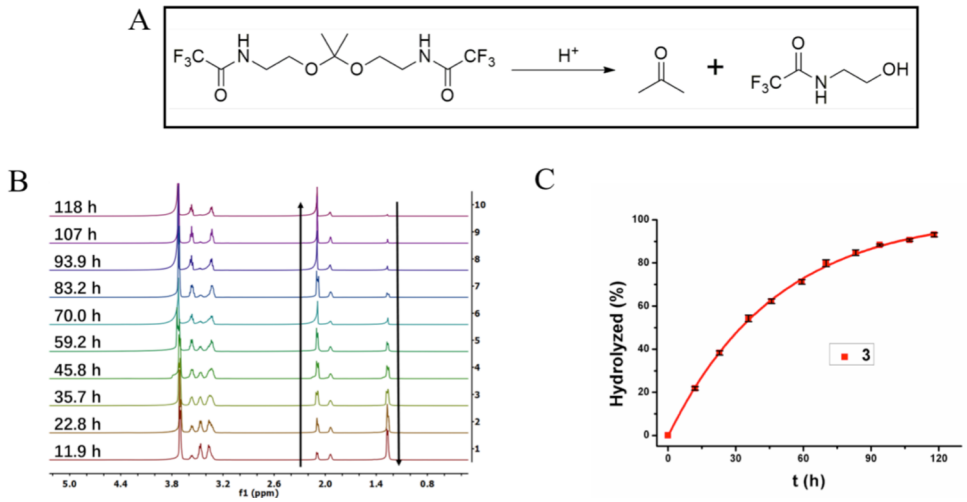

Figure 3. Hydrolysis of molecule **3** at pH 5 conditions. (A) Hydrolysis reaction studied, (B) NMR spectra of the hydrolytic process, (C) hydrolysis kinetics together with the first-order reaction fitting curve (solid line).

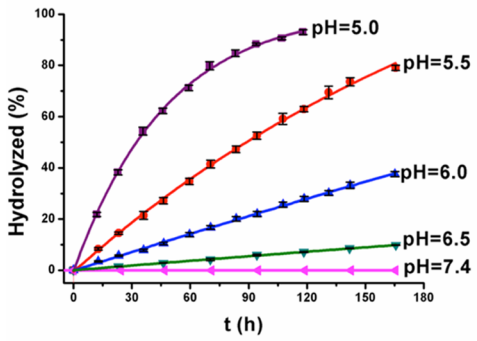

pH	$t_{1/2}$ (h)
5.0	32.33±0.90
5.5	88.83±3.43
6.0	222.04±4.24
6.5	1222.2±71.0
7.4	-

Figure 4. Relative hydrolysis kinetics of ketal **3** at different pH. The solid lines are the fitting curves.

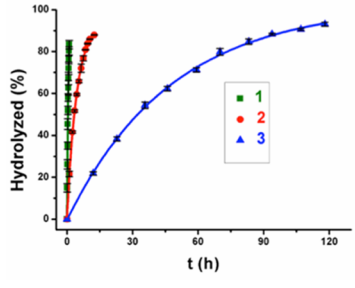

	Structure	$t_{1/2}$ (h)
1	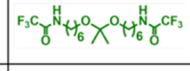	0.40±0.03
2	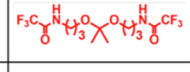	3.26±0.09
3	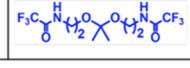	32.33±0.90

Figure 5. Relative hydrolysis rates of ketals based on the variation in the distance between the electron-withdrawing amide moiety and ketal moiety at pH 5 conditions. The solid lines are the fitting curves.

of placing an electron-withdrawing group close to the carboxonium ion intermediate (Figure 5). The half-life of ketal **1**, formed between acetone and the amide derivative 6-amino-hexan-1-ol, was found to be about 24 min. When the six-carbon linker was changed to only three carbons in **2**, the half-life of the ketal increased by about 1 order of magnitude to more than 3 h, indicating substantial increase in stability. This increased stability is attributed to the closer proximity between the amide and the ketal moieties. Interestingly, when the linker length was decreased by one more carbon in **3**, the half-life increased by yet another order of magnitude to about 32 h. The greater sensitivity at shorter distances is the classic hallmark of inductive effect based destabilization of the carboxonium ion intermediate, which understandably raises the transition state energy.

Next, the effect of the intermediate being a primary, secondary or tertiary carboxonium ion upon the rate of hydrolysis was investigated (Series B in Figure 2). In this case, molecules **4**, **5**, and **6** were synthesized from the reaction of the phthalimide derivative of 2-amino-ethanol and acetone, acetaldehyde, and formaldehyde, respectively. Phthalimides were used as the protecting group in this series because of experimental difficulties in synthesizing the corresponding trifluoroacetamide derivatives. Also, the electron-withdrawing ability of these two amino protecting groups were also found to be similar. The hydrolytic half-life of the phthalimide-

DOI: 10.1021/jacs.6b11181
J. Am. Chem. Soc. 2017, 139, 2306−2317

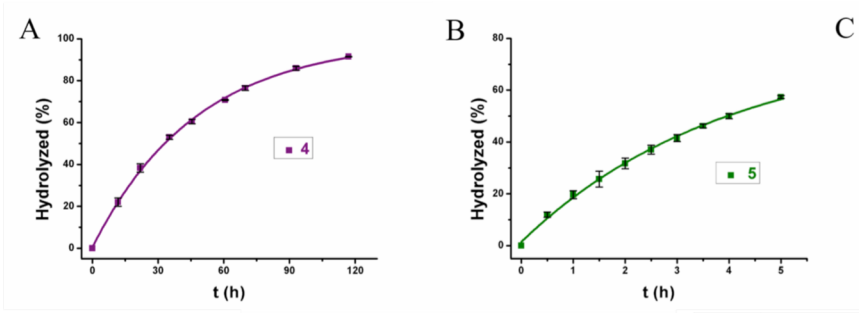

	Structure	$t_{1/2}$
4		32.96±1.25 h[i]
5	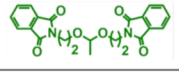	3.96±0.11 h[ii]
6	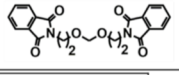	-

	Structure	$t_{1/2}$ (h)
5	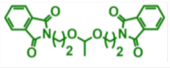	3.96±0.11
7		4.11±0.08
8	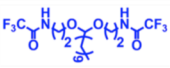	4.16±0.23

Figure 6. (A–C) Effect of the primary, secondary, or tertiary carboxonium ion as the intermediate species upon the hydrolysis rates of acetals and ketals. A and i were under pH = 5 buffer conditions; B and ii were under TFA conditions. (D and E) Effect of alkyl chain length upon the stability of secondary carboxonium ions under TFA conditions. The solid lines are the fitting curves.

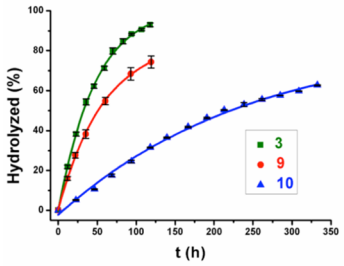

	Structure	$t_{1/2}$ (h)
3	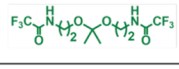	32.33±0.90
9		51.35±3.89
10	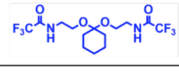	221.17±2.15

Figure 7. Relative hydrolysis rates of ketals from acyclic vs cyclic ketones at pH 5. The solid lines are the fitting curves.

substituted ketal **4** was found to be about 33 h (Figure 6A), which is very similar to that of the corresponding trifluoroacetamide-substituted ketal **3** ($t_{1/2}$ = 32.33 ± 0.90 h). Within the Series B, the two acetals, **5** and **6**, were too inert to be studied at the pH 5 conditions used for **4**. Therefore, the reaction was carried out in the presence of trifluoroacetic acid (TFA), and the results are shown in Figure 6B,C. Under these conditions, a mixture of 0.3 mL of CD_3CN and 0.1 mL of 50 mM TFA in D_2O was used as the solvent, where the concentration of the molecules under investigation was also kept at 25 mM. Even under these conditions, the formaldehyde acetal moiety in **6** did not show any degradation, suggesting that the barrier for the formation of the formal primary carboxonium ion is quite high. On the other hand, the half-life of the acetal from acetaldehyde in **5** was found to be about 4 h.

Because the alkylidene acetals showed any appreciable cleavage only in the presence of TFA, these conditions were also used to investigate the effect of alkyl chains upon the hydrolysis kinetics (Series C). Not surprisingly, the alkyl chain length did not have any appreciable effect on the hydrolysis rate (Figure 6D,E).

Similarly, the effect of alkyl group variations in ketals was also investigated by comparing ketals formed from acetone, cyclopentanone, and cyclohexanone at pH 5. Although all three molecules are ketals and therefore result in a tertiary carboxonium intermediate, the half-lives were found to be substantially different. Hydrolysis rate of the cyclopentyl ketal was found to be about two times slower, whereas that of cyclohexanone was about seven times slower, compared to the acetone analog. The difference between the five- and the six-membered ring can be attributed to the difference in torsional energy strain between the ground state and the transition state in the reaction.[24]

Although secondary carboxonium intermediates exhibit slow hydrolysis rates, we were interested in understanding the effect of replacing the alkyl substituent with an aryl moiety. The placement of the aryl moiety also provides the opportunity to more reliably probe the effect of electron-withdrawing and electron-donating substituents upon the stability of the carboxonium ion and thus on the hydrolysis rates of the acetals. The results of these findings are shown in Figure 8. Briefly, benzylidene acetals that are unsubstituted or substituted with electron-withdrawing functionalities, exhibit slow hydrolysis under the pH 5 conditions. Therefore, these experiments were carried out in the presence of TFA. Under these conditions, the half-life of the phenyl-substituted acetal **13** was found to be about 4 min. Incorporating a trifluoromethyl moiety, an inductively electron-withdrawing group, at the para

DOI: 10.1021/jacs.6b11181
J. Am. Chem. Soc. 2017, 139, 2306–2317

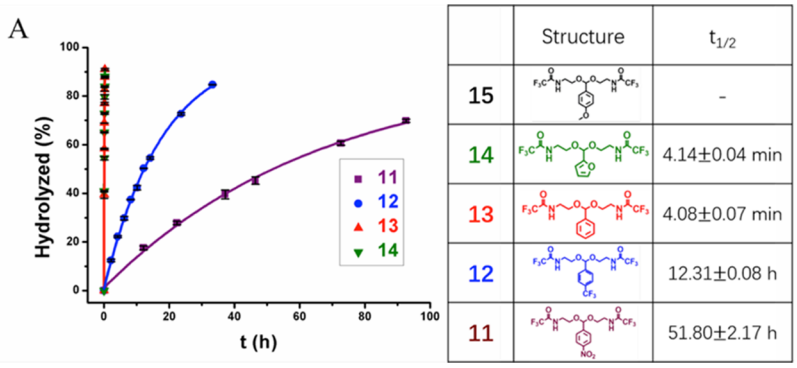

	Structure	$t_{1/2}$
15		-
14		4.14±0.04 min
13		4.08±0.07 min
12		12.31±0.08 h
11		51.80±2.17 h

Figure 8. Substituent effects upon the hydrolysis of benzylidene acetals. (A) Hydrolysis kinetics and the first-order reaction fitting curve, (B) Hammett plot. The hydrolysis was performed under TFA condition. The solid lines are the fitting curves.

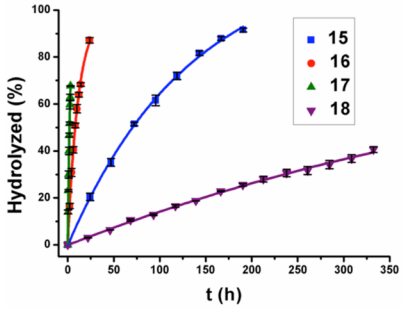

	Structure	$t_{1/2}$ (h)
17		1.84±0.07
16		7.98±0.30
15		70.42±1.17
18		425.0±15.2

Figure 9. Effect of varying the number and position of the electron-donating methoxy substituents upon the hydrolysis of benzylidene acetals at pH 5 conditions. The solid lines are the fitting curves.

Table 1. Relative Hydrolysis Rates of the Acetal/Ketals Used in This Study

6	11	12	8	7	5
-	$1.31*10^{-3}$x	$5.52*10^{-3}$x	$1.63*10^{-2}$x	$1.65*10^{-2}$x	$1.72*10^{-2}$x
13	14	18	10	15	9
1x	~1x	5.26x	10.11x	31.75x	43.53x
4	3	16	2	17	1
67.82x	69.15x	$2.80*10^{2}$x	$6.86*10^{2}$x	$1.21*10^{3}$x	$5.59*10^{3}$x

position in **12** reduced the half-life by 2 orders of magnitude to about 12.3 h. The presence of a resonance-based electron-withdrawing group in **11** reduced the half-life by another 4 times. Interestingly, furan-based acetal **14** seems to behave very similar to the unsubstituted benzylidene acetal **13**. Incorporating an electron-donating *p*-methoxy moiety in **15** greatly enhanced the rate of hydrolysis in that the reaction was too fast to be measured under these conditions. By comparison, the half-life of acetal **15** under pH 5 conditions was found to be about 70.4 h. To bridge the gap for the two different hydrolytic conditions, the reduced TFA amount (1/5 of the initial amount) was used for the hydrolytic study. For instance, a mixture of 0.3 mL of CD_3CN and 0.1 mL of 10 mM TFA in D_2O was used as the solvent and the concentration of the molecules under investigation was also kept at 25 mM. In this case, molecule **13** showed a half-life of 4.08 min under typical TFA conditions (Figure 7); however, it revealed the half-life of 25.33 min under these reduced TFA conditions (Figure S3). It meant the reaction rate decreased by about 6 times under the milder acidic conditions. Further, acetal **18** has a half-life of 4.82 min under reduced TFA condition (Figure S3), but it is increased to 425 h (Figure 8) under the pH = 5 buffer condition, suggesting that the difference in reaction rate between these two conditions is about 5.29×10^3. Based on these, the reaction rate under our typical TFA conditions is about 3.28×10^4 times faster than that under pH 5 buffer

DOI: 10.1021/jacs.6b11181
J. Am. Chem. Soc. 2017, 139, 2306−2317

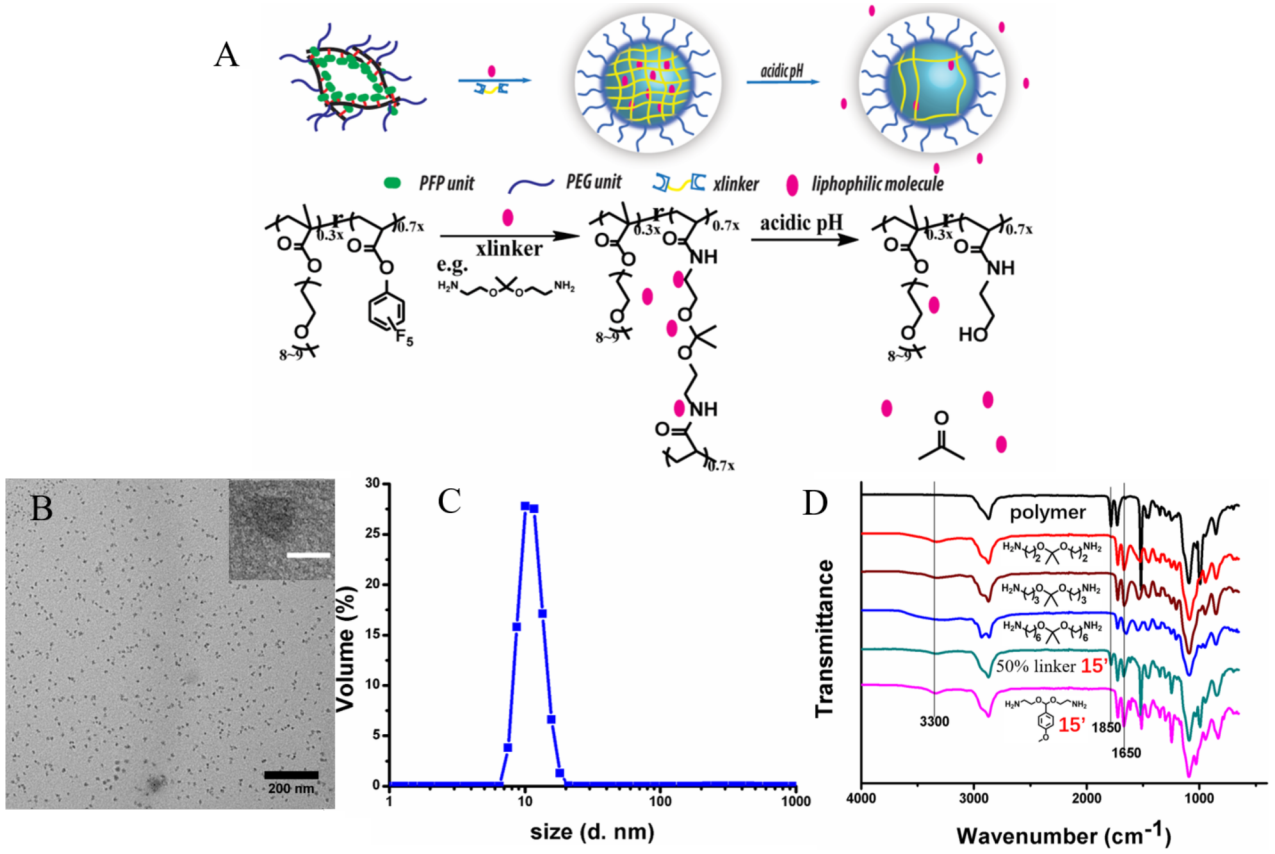

Figure 10. Preparation and characterization of the nanogels: (A) synthesis of the nanogels, (B) TEM image of the nanogels from cross-linker **3′** (inset figure is magnified TEM image, scale bar = 20 nm), (C) DLS of the nanogels from cross-linker **3′**, (D) IR spectrum of the nanogels from different cross-linkers.

conditions. Thus, the hydrolytic rate for acetal **15** is estimated to be ∼32 times faster than that of acetal **13**. As all reactions showed very good first-order reaction kinetics, the reaction rate constant k equals $0.693/t_{1/2}$. A Hammett plot with **11**, **12**, **13**, and **15** from $\log(k/k_0)$ vs σ value[46] of the substituents on the phenyl ring yielded ρ value of −4.06 ($R^2 > 0.99$), as shown in Figure 8B. The reasonably high negative ρ value shows the importance of stabilizing the carboxonium ion intermediate in these molecules to accelerate the degradation.

Because acetal **15** did exhibit reasonable hydrolysis rates at pH 5, we further probed the effect of varying the number and position of methoxy moieties in the aryl moiety. Accordingly, when the number of methoxy moieties were increased to two, where these functionalities were incorporated at the para and the ortho positions in **16**, the hydrolysis rate increased by an order of magnitude. The half-life decreased for **16** to ∼8 h, compared to ∼70 h for **15**. Adding one more methoxy moiety to the other ortho position in **17** decreased the half-life even further to about 1.8 h. Interestingly, when the substitution pattern is changed from 2,4,6-trimethoxy to 3,4,5-trimethoxy units, the hydrolysis rate decreased by more than 2 orders of magnitude to ∼425 h. This is attributed to the fact that the methoxy units at the meta positions behave more as an inductively electron-withdrawing moiety with respect to the carboxonium ion. The results of these findings are shown in Figure 9.

Based on all the kinetics of the different acetal/ketal molecules, the relative hydrolytic kinetics is summarized and shown in Table 1. The relative hydrolysis rates are tabulated with the unsubstituted benzylidene acetal **13** as the standard. Based on the cross-correlations mentioned above, where the same molecule has been subjected to different degradation conditions, all these relative rates have been estimated as rates under the pH 5 conditions. The data in Table 1 show that the relative hydrolysis rates of the acetal/ketal molecules can be varied by nearly 7 orders of magnitude by judiciously choosing the substituents. In addition to the range provided by the substituents studied here, one can also imagine using the structure−property correlations here to expand logically this range even further.

Because the inspiration behind the construction of most pH-sensitive materials is driven by the possible utility in biological applications such as drug delivery and sensing, we were interested in testing whether there is a correlation between the kinetics of hydrolysis of small molecule acetals and the behavior of the same in nanomaterials. By designing acetal- and ketal-containing nanomaterials that are capable of acting as hosts for noncovalently bound guest molecules, we were especially interested in understanding the evolution of the fidelity of these nanomaterials as hosts at different pH values. We design nanogels, prepared by a recently reported emulsion-free method,[44,45] that are capable of sequestering hydrophobic guest molecules. In addition to simply correlating the small molecule degradation with encapsulation in polymeric nanoparticles, we also envisage that this study is important because the microenvironments of these functionalities in the nanogels are different from those in the bulk solution studied above with small molecules.

DOI: 10.1021/jacs.6b11181
J. Am. Chem. Soc. 2017, 139, 2306−2317

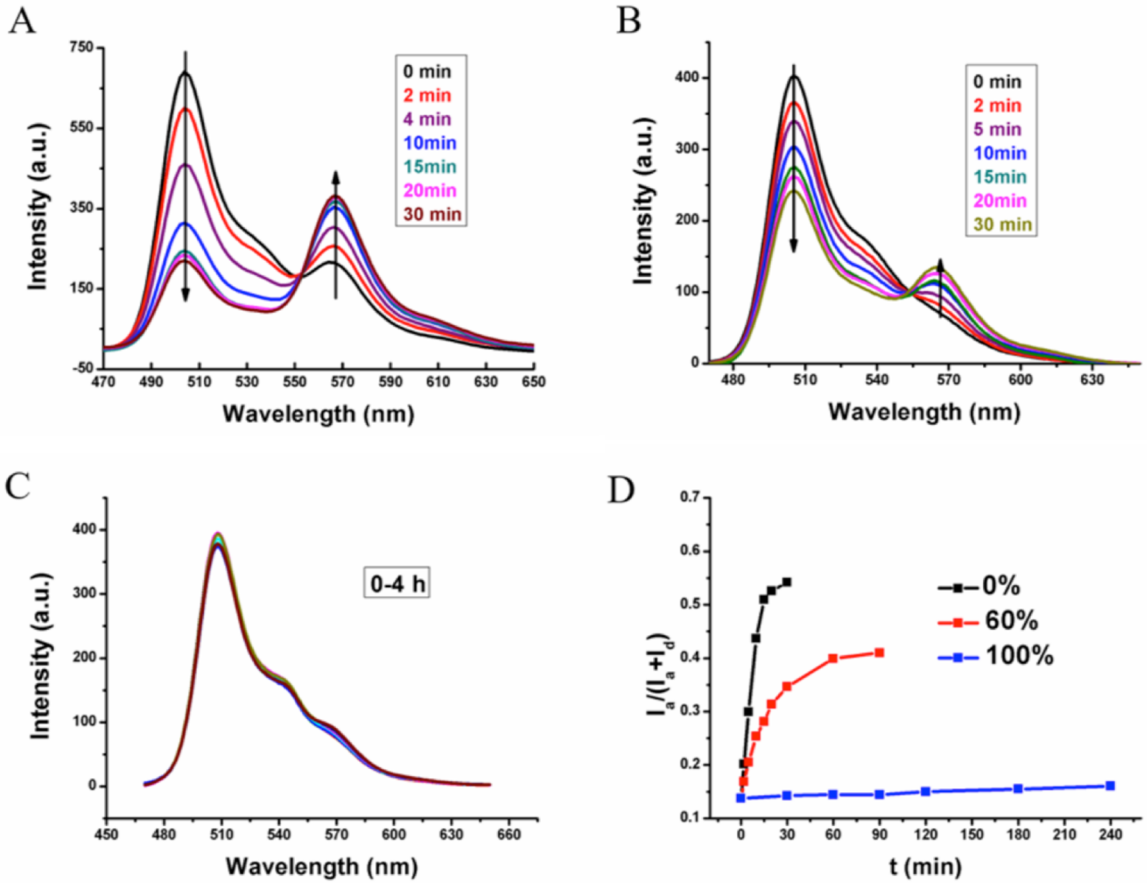

Figure 11. Encapsulation stability of the nanogels under different cross-link degree at pH = 7.4. (A) 0%, (B) 60%, (C) 100%; (D) FRET ratio change with time.

An amphiphilic random copolymer precursor was first prepared, where the hydrophilic monomer contained a PEG moiety as the hydrophilic side chain and the hydrophobic monomer was based on the reactive pentafluorophenyl ester (PFPE) moiety. The amphiphilic polymer can self-assemble in aqueous phase to form a nanoscopic amphiphilic aggregate, which was used as the template for the nanogels. The active PFPE groups on the amphiphilic polymer can readily react with amine groups of the pH-sensitive linker, generated by deprotecting the trifluoroacetyl protecting groups in Figure 2, to cross-link the micellar aggregates in water through the amidation (Figure 10A). The structures of the deprotected linkers are shown in Figure S2, the numbers of which correspond to the protected precursor molecules with a prime on the number. The cross-linking process was conveniently monitored by FT-IR as shown in Figure 10D. The activated carbonyl group in PFPE of the polymer precursor exhibits a strong, characteristic peak at 1850 cm^{-1}. Upon amidation based cross-linking, this peak disappears with the concurrent appearance of new peaks at ∼1650 and at 3300 cm^{-1}, attributed to the carbonyl and the N−H functionalities of the amide moiety, respectively. We found this reaction to be nearly quantitative in all cases. When 0.5 equiv of a linker was used for reaction, the peak attributed to the activated ester completely disappears, accompanied by the appearance of a strong peak for the amide moiety. We assume that this represents >95% cross-linking in these nanogels. Similarly, if only 0.25 equiv of the linker was consumed, the peak intensity for the activated ester decreased to about half of the original precursor polymer. The quantitative nature of this cross-linking reaction, with all cross-linkers studied, facilitates comparisons between different cross-linkers. Also, because the precursor polymer assembly size determines the size of the cross-linked polymer nanogel in these cases, sizes of the nanogel in all these variations were also quite consistent. Size of the nanogel was found to be ∼10 nm both by dynamic light scattering (DLS) and transmission electron microscopy (TEM) as exemplified in Figure 10 and Figure S5.

Encapsulation stability can be most rigorously defined as a measure of the dynamic exchange of the encapsulated guest molecules with the bulk solvent and thus with another nanogel present in solution.[47] We use the previously established fluorescence resonance energy transfer (FRET) method to interrogate this dynamics.[47] Briefly, a pair of hydrophobic FRET dyes (3,3′-dioctadecyloxacarbocyanine perchlorate (DiO, donor) and 1,1′-dioctadecyl-3,3,3′,3′-tetramethylindocarbocyanine perchlorate (DiI, acceptor)) are incorporated as guests into two separate nanogels. When aqueous solutions of these two nanogels are mixed, the dye molecules will stay within their respective nanogels without any temporal evolution of FRET, if the encapsulation stability were very high. On the other hand, if the encapsulation stability were low, there would be a temporal evolution of the donor and acceptor fluorescence. The kinetics of this evolution is directly related to the magnitude of encapsulation stability, which is defined as the leakage coefficient (Λ) for supramolecular assemblies.

As shown in Figure 11A, the guest exchange was faster when the precursor polymer was used as the host without any cross-

DOI: 10.1021/jacs.6b11181
J. Am. Chem. Soc. 2017, 139, 2306−2317

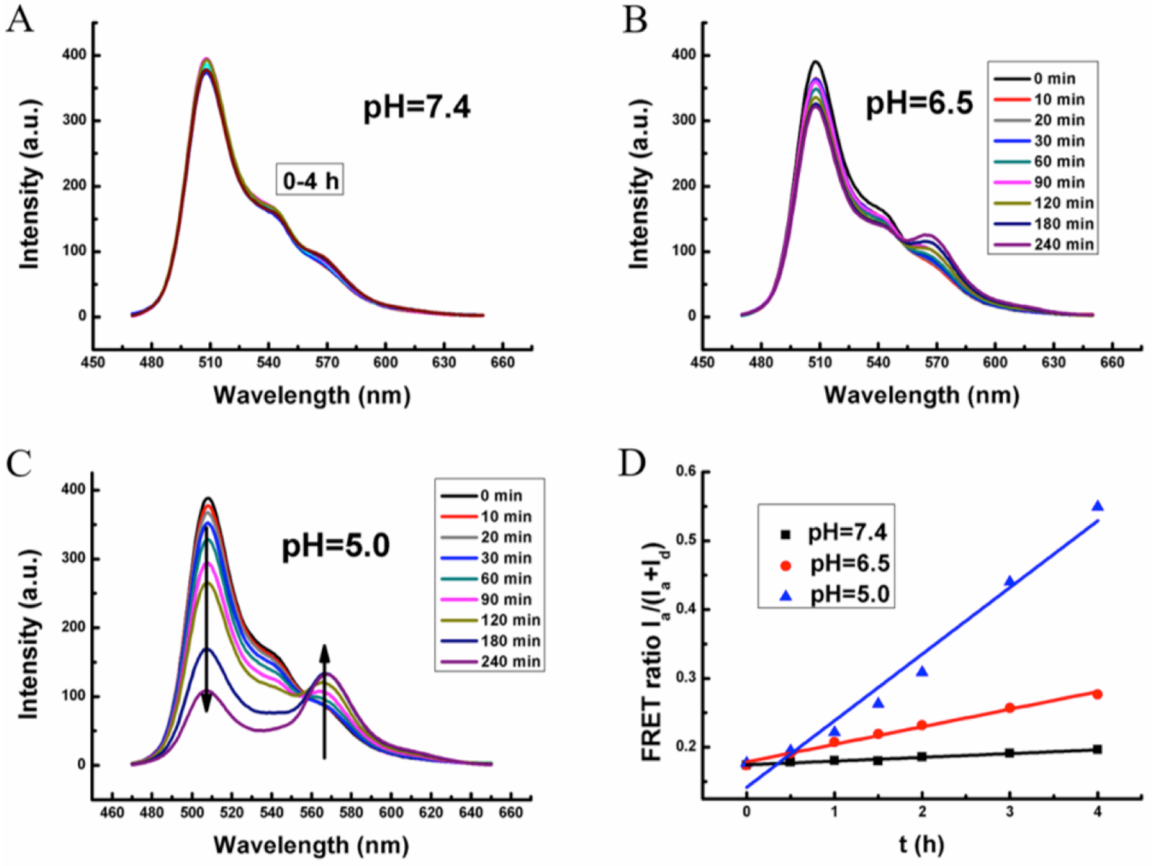

Figure 12. pH-dependent variations in exchange dynamics of the nanogel **N3**, derived from the cross-linker **3′** or **4′** based on the ketal **3** and **4**. The solid lines in panel D are the linear fitting curves.

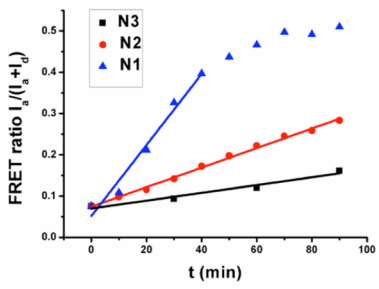

	Linker structure	Leakage coefficient (Λ)
N1	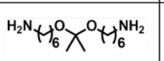	0.52 h^{-1}
N2	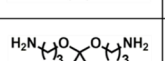	0.15 h^{-1}
N3	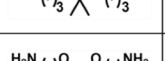	0.087 h^{-1}

Figure 13. Effect of varying the distance between the electron-withdrawing amide moiety and ketal moiety upon guest encapsulation stability in nanogels **N1**−**N3**. The solid lines in the figure are the linear fitting curves.

linking, where the emission of the donor peak at 508 nm decreases and the emission peak of the acceptor at 568 nm increases with time. This suggests that this assembly is quite leaky. Upon cross-linking the assembly with 0.3 equiv of cross-linker **3′**, the 60% cross-linked nanogel was less leaky, whereas the FRET ratio for the 100% cross-linked nanogel did not change with time. This supports the idea that the uncross-linked micelle-like assemblies are quite leaky, but the encapsulation stability can be substantially increased with cross-linking. In all the subsequent studies that vary the structure of the acetal or ketal based cross-linkers, 100% cross-linking was used. This degree of cross-linking was targeted to (a) rule out the possibility of change in encapsulation stability due to the slow hydrolysis of PFP moieties; (b) ensure high intrinsic stability of the nanogels in the absence of pH-induced cleavage of the acetal- or ketal-based cross-linkers.

Because the acetone-based ketal provides reasonable susceptibility to pH, linker **3′** was first used for the preparation of the nanogels to monitor the difference in encapsulation stability upon varying the pH of the solution. As shown in Figure 12A,B, although there is no FRET evolution at pH 7.4, indicative of high encapsulation stability, the nanogel becomes leaky at pH 6.5. The leakage coefficient at pH 6.5 was found to be 0.026 h^{-1}, compared to ∼0 at pH 7.4 (Figure 12D). This leakage increased further at pH 5 to 0.087 h^{-1}, supporting the assertion that the pH-dependent ketal degradation kinetics can directly affect the encapsulation stability of the nanogel. To compare the relative effects of pH-induced cleavage upon the nanogel's encapsulation stability, we evaluated FRET evolution of nanogels containing different acetal- or ketal-based cross-linkers at pH 5. Accordingly, we tested the nanogels made of the cross-linkers derived from ketals shown in Series A in

DOI: 10.1021/jacs.6b11181
J. Am. Chem. Soc. 2017, 139, 2306−2317

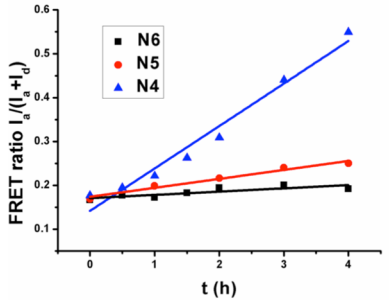

	Linker structure	Leakage coefficient (Λ)
N4	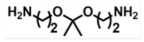	0.087 h^{-1}
N5	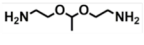	0.019 h^{-1}
N6	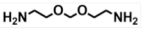	0 h^{-1}

Figure 14. Effect of the primary, secondary, or tertiary carboxonium ion as the intermediate species upon the encapsulation stability in nanogels **N4**–**N6**. The solid lines in the figure are the linear fitting curves.

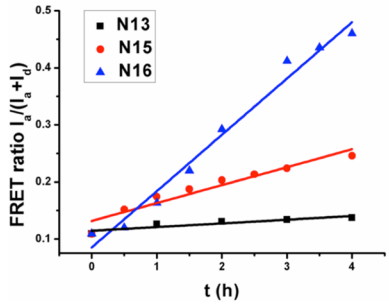

	Linker structure	Leakage coefficient (Λ)
N13	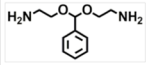	0.007 h^{-1}
N15	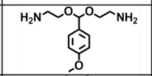	0.034 h^{-1}
N16	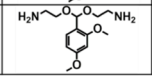	0.101 h^{-1}

Figure 15. Substituent effects in benzylidene acetal-based nanogels, **N13**, **N15** and **N16**, upon their guest encapsulation stability. The solid lines in the figure are the linear fitting curves.

Figure 2, where the effect of the electron-withdrawing amide moiety is tested. As shown in Figure 13, the distance between the pH-sensitive ketal moiety and the electron-withdrawing amide moiety does indeed affect the encapsulation stability. The leakage coefficient for the nanogel **N1** with a C6 linker was found to be 0.52 h^{-1}, whereas it was found to be 0.15 and 0.087 h^{-1} for **N2** and **N3**, respectively. Two factors, which could potentially complicate the interpretation that the electron-withdrawing nature of the substituents are the key players in this series, should be considered: (i) The increased distance between ketal and the amide also increases the length of the cross-linker, which could make the nanogel based on **1′** to exhibit less encapsulation stability. Although possible, this is less likely to be a factor, because all three nanogels displayed no leakage at pH 7.4, where ketal degradation is not expected to occur. (ii) The C6-cross-linker in **1′** endows the nanogel with a more hydrophobic interior, compared to the C2-cross-linker in **3′**. In this case, the encapsulation stability is expected to be higher for **N1**, compared to **N3**. However, the opposite trend is observed, which is consistent with the hydrolysis kinetics of the small molecule ketal.

To test further whether the hydrolysis kinetics of the small molecules correlate with the encapsulation stability in the nanogels, we tested Series B, where the linker lengths are identical, but the stability of the carboxonium ions vary significantly. Indeed the formaldehyde acetal, which did not exhibit any cleavage as a small molecule in **6**, did not seem to degrade in the nanogel **N6** either as the leakage coefficient was found to be close to zero (Figure 14). On the other hand, the nanogel **N5** based on the acetaldehyde-acetal exhibits slow change in encapsulation stability with a leakage coefficient of 0.019 h^{-1}, whereas the FRET evolution was much faster in **N4** (same as **N3** in the nanogel) with a leakage coefficient of 0.087 h^{-1}.

Once again, the small molecule hydrolytic stability seems to correlate qualitatively with the encapsulation stability in the nanogels. Note however that the difference in the hydrolytic rate constants between **4** and **5** is more than 3 orders of magnitude, whereas the leakage coefficient is different by only four to five. Similar correlations were also found for the nanogels synthesized from Series D (see SI for details).

Finally, we explored the effect of substituents in benzylidene acetals on the guest encapsulation stability of the corresponding nanogels. In Series E and F, the aryl moieties that contain electron-withdrawing moieties were too slow to be monitored through the FRET exchange studies. Therefore, we studied the phenyl- (**N13**) and compared them with methoxy-substituted nanogels, **N15** and **N16**. Once again, the trend in encapsulation stability, shown in Figure 15, was consistent with that found with small molecules. Interestingly, there was a small difference in encapsulation stability between the phenyl-substituted and furan-substituted nanogels, whereas such a difference did not exist in the case of small molecules (Figure S9). This small difference is attributed to the fact that the furan ring is considered to be a bit more hydrophilic compared to the phenyl ring, which is likely playing a role in the encapsulation stability of these nanogels.

CONCLUSION

In summary, a series of acetal- and ketal-based molecules have been synthesized and evaluated for their pH-sensitive degradation properties. Upon studying six different series of these molecules, we arrive at the following conclusions: (i) Hammett correlations of substituted benzylidene acetals show that the ρ value for the degradation reaction is about −4.06. This shows that there is a strong positive charge development in the transition state of this acid-catalyzed degradation process. Although it is anticipated that an acid-catalyzed process would have a developing positive charge, the large magnitude of this

DOI: 10.1021/jacs.6b11181
J. Am. Chem. Soc. 2017, 139, 2306–2317

influence was certainly surprising. As a point of comparison, the ρ^+ value for the solvolysis of cumyl chloride is −4.45,[48] which is considered to be an S_N1-like process, supporting the strong developing positive charge at the benzylic position in the transition state in acetal degradation. (ii) The relative positioning of the ketal moiety and the electron-withdrawing amido group can greatly influence its degradation, in that there is a 2 orders of magnitude difference in the cleavage rates of 2- and 6-carbon linkers. (iii) Acetal derivatives of formaldehyde and acetaldehyde, and the ketal derivative of acetone, have substantially different reactivities, presumably due to the variations in stabilities of 1°, 2°, and 3° carboxonium ion type intermediates. (iv) Understandably, the length of the alkyl chain substituents in the acetal carbon did not have a substantial influence upon the stability of carboxonium ion stability and thus the rates of acetal hydrolysis. (v) Comparison of ketals derived from acetone, cyclopentanone, and cyclohexanone shows that torsional effects also have substantial influence upon the degradation kinetics. (vi) Incorporation of these functional groups as cross-linkers within polymeric nanogels causes them to exhibit pH-sensitive host−guest properties. Studying the effect of variations in the structure of the cross-linker upon the encapsulation stability of the nanogels at lower pH reveals that the trends observed in the small molecule degradation faithfully translate to the host−guest properties in the nanogels.

Overall, the study outlined here provides a comprehensive overview of structural variations that afford the opportunity to tune the pH-sensitivity of acetal- and ketal-based linkers. We show that the structural fine-tuning of the linkers allows access to variations in kinetics of degradation of more than 6 orders of magnitude. The effect of structural variations upon the pH-sensitive host−guest characteristics of polymeric nanogels constitutes one such example. The overall impact of this fundamental study is likely to be much broader in a variety of applications, including drug delivery and tissue engineering.[49−52] Utilizing these findings in biosensing and drug delivery applications includes part of the future efforts in our own laboratories.

EXPERIMENTAL SECTION

Most of the experimental details are presented in the Supporting Information. Three of the key procedures are outlined here.

Hydrolytic Study of the Acetal/Ketal. 0.01 mmol of the acetal/ketal molecules was dissolved in 0.3 mL of CD_3CN, and then 0.1 mL of PB D_2O buffer (0.2 M, pH = 5) was added for hydrolysis. The corresponding hydrolytic process was monitored by 400 MHz NMR at room temperature. The fast hydrolytic study was performed with acid as the catalyst. 0.01 mmol of the acetal/ketal molecule was dissolved in 0.3 mL of CD_3CN, and then 0.1 mL of CF_3COOH solution (in D_2O, 50 mM) was added for hydrolysis. The reduced TFA hydrolytic condition was similar except using 0.1 mL of 10 mM CF_3COOH solution (in D_2O).

Preparation of the Nanogels. 10 mg of polymer was dissolved in 1 mL of pH = 7.4 buffer. Then, the cross-linker (11.33 μmol for 100% cross-link degree) and 4 μL of DIPEA were added under stirring for another 24 h. The solution was further purified through dialysis under PBS buffer. If the nanogels were used to load dyes inside, the stock solution of the dye was added into the polymer solution before the addition of the cross-linker and DIPEA. The final nanogels were stored in PBS solution with the concentration of 2 mg/mL.

FRET Study with the Nanogels. The FRET study was performed by the mixture of the DiI loaded nanogels and DiO loaded nanogels under different pH. 0.1 mL DiI loaded nanogels and 0.1 mL DiO loaded nanogels were mixed in the presence of 0.8 mL buffer (0.2 M) with different pH values. The fluorescence of the solution was recorded with the excitation wavelength of 450 nm.

Data Analysis. All the hydrolysis experiments were performed three times. The error values for $t_{1/2}$ were reported as the standard deviations of the three trials. The data points and error bars in the figures represent the average and standard deviation at each data point, respectively. The solid lines are the exponential fitting curve of the data points.

ASSOCIATED CONTENT

Supporting Information

The Supporting Information is available free of charge on the ACS Publications website at DOI: 10.1021/jacs.6b11181.

Experimental details, Figures S1−S10, and Table S1−2 (PDF)

AUTHOR INFORMATION

Corresponding Author

*thai@chem.umass.edu

ORCID

S. Thayumanavan: 0000-0002-6475-6726

Notes

The authors declare no competing financial interest.

ACKNOWLEDGMENTS

We thank support from the Army Research Office (W911NF-15-1-0568) and National Institutes of Health (CA-169140) for support.

REFERENCES

(1) Stuart, M. A. C.; Huck, W. T. S.; Genzer, J.; Müller, M.; Ober, C.; Stamm, M.; Sukhorukov, G. B.; Szleifer, I.; Tsukruk, V. V.; Urban, M.; Winnik, F.; Zauscher, S.; Luzinov, I.; Minko, S. *Nat. Mater.* **2010**, *9*, 101−113.

(2) Mura, S.; Nicolas, J.; Couvreur, P. *Nat. Mater.* **2013**, *12*, 991−1003.

(3) Roy, D.; Cambre, J. N.; Sumerlin, B. S. *Prog. Polym. Sci.* **2010**, *35*, 278−301.

(4) Casey, J. R.; Grinstein, S.; Orlowski, J. *Nat. Rev. Mol. Cell Biol.* **2010**, *11*, 50−61.

(5) Izumi, H.; Torigoe, T.; Ishiguchi, H.; Uramoto, H.; Yoshida, Y.; Tanabe, M.; Ise, T.; Murakami, T.; Yoshida, T.; Nomoto, M.; Kohno, K. *Cancer Treat. Rev.* **2003**, *29*, 541−549.

(6) Maxfield, F. R.; McGraw, T. E. *Nat. Rev. Mol. Cell Biol.* **2004**, *5*, 121−132.

(7) Grant, B. D.; Donaldson, J. G. *Nat. Rev. Mol. Cell Biol.* **2009**, *10*, 597−608.

(8) Yamagata, M.; Hasuda, K.; Stamato, T.; Tannock, I. F. *Br. J. Cancer* **1998**, *77*, 1726−1731.

(9) Helmlinger, G.; Schell, A.; Dellian, M.; Forbes, N. S.; Jain, R. K. *Clin. Cancer Res.* **2002**, *8*, 1284−1291.

(10) Vander Heiden, M. G.; Cantley, L. C.; Thompson, C. B. *Science* **2009**, *324*, 1029−1033.

(11) Webb, B. A.; Chimenti, M.; Jacobson, M. P.; Barber, D. L. *Nat. Rev. Cancer* **2011**, *11*, 671−677.

(12) Ma, X.; Wang, Y.; Zhao, T.; Li, Y.; Su, L.; Wang, Z.; Huang, G.; Sumer, B. D.; Gao, J. *J. Am. Chem. Soc.* **2014**, *136*, 11085−11092.

(13) Kim, H. K.; Shim, W. S.; Kim, S. E.; Lee, K.-H.; Kang, E.; Kim, J.-H.; Kim, K.; Kwon, I. C.; Lee, D. S. *Tissue Eng., Part A* **2009**, *15*, 923−933.

(14) Bae, Y.; Nishiyama, N.; Kataoka, K. *Bioconjugate Chem.* **2007**, *18*, 1131−1139.

(15) Liu, J.; Huang, Y.; Kumar, A.; Tan, A.; Jin, S.; Mozhi, A.; Liang, X. *Biotechnol. Adv.* **2014**, *32*, 693−710.

DOI: 10.1021/jacs.6b11181
J. Am. Chem. Soc. 2017, 139, 2306−2317

(16) Binauld, S.; Stenzel, M. H. *Chem. Commun.* **2013**, *49*, 2082−2102.
(17) Gao, W.; Chan, J. M.; Farokhzad, O. C. *Mol. Pharmaceutics* **2010**, *7*, 1913−1920.
(18) Kamaly, N.; Yameen, B.; Wu, J.; Farokhzad, O. C. *Chem. Rev.* **2016**, *116*, 2602−2663.
(19) Bielski, R.; Witczak, Z. *Chem. Rev.* **2013**, *113*, 2205−2243.
(20) Leriche, G.; Chisholm, L.; Wagner, A. *Bioorg. Med. Chem.* **2012**, *20*, 571−582.
(21) Zhang, X.; Malhotra, S.; Molina, M.; Haag, R. *Chem. Soc. Rev.* **2015**, *44*, 1948−1973.
(22) Cordes, E. H.; Bull, H. G. *Chem. Rev.* **1974**, *74*, 581−603.
(23) Fife, T. H. *Acc. Chem. Res.* **1972**, *5*, 264−272.
(24) Kreevoy, M. M.; Morgan, C. R.; Taft, R. W. *J. Am. Chem. Soc.* **1960**, *82*, 3064−3066.
(25) Murthy, N.; Thng, Y. X.; Schuck, S.; Xu, M. C.; Fréchet, J. M. J. *J. Am. Chem. Soc.* **2002**, *124*, 12398−12399.
(26) Griset, A. P.; Walpole, J.; Liu, R.; Gaffey, A.; Colson, Y. L.; Grinstaff, M. W. *J. Am. Chem. Soc.* **2009**, *131*, 2469−2471.
(27) Wang, L.; Liu, G. H.; Wang, X. R.; Hu, J. M.; Zhang, G. Y.; Liu, S. Y. *Macromolecules* **2015**, *48*, 7262−7272.
(28) Hong, B. J.; Chipre, A. J.; Nguyen, S. T. *J. Am. Chem. Soc.* **2013**, *135*, 17655−17658.
(29) Paramonov, S. E.; Bachelder, E. M.; Beaudette, T. T.; Standley, S. M.; Lee, C. C.; Dashe, J.; Fréchet, J. M. J. *Bioconjugate Chem.* **2008**, *19*, 911−919.
(30) Jain, R.; Standley, S. M.; Fréchet, J. M. J. *Macromolecules* **2007**, *40*, 452−457.
(31) Shenoi, R. A.; Narayanannair, J. K.; Hamilton, J. L.; Lai, B. F. L.; Horte, S.; Kainthan, R. K.; Varghese, J. P.; Rajeev, K. G.; Manoharan, M.; Kizhakkedathu, J. N. *J. Am. Chem. Soc.* **2012**, *134*, 14945−14957.
(32) Chatterjee, S.; Ramakrishnan, S. *Macromolecules* **2011**, *44*, 4658−4664.
(33) Liu, N.; Vignolle, J.; Vincent, J. M.; Robert, F.; Landais, Y.; Cramail, H.; Taton, D. *Macromolecules* **2014**, *47*, 1532−1542.
(34) Bachelder, E. M.; Beaudette, T. T.; Broaders, K. E.; Dashe, J.; Fréchet, J. M. J. *J. Am. Chem. Soc.* **2008**, *130*, 10494−10495.
(35) Li, Y. L.; Du, W. J.; Sun, G. R.; Wooley, K. L. *Macromolecules* **2008**, *41*, 6605−6607.
(36) Shim, M. S.; Kwon, Y. J. *Polym. Chem.* **2012**, *3*, 2570−2577.
(37) Gillies, E. R.; Goodwin, A. P.; Fréchet, J. M. J. *Bioconjugate Chem.* **2004**, *15*, 1254−1263.
(38) Clark, A. J.; Davis, M. E. *Proc. Natl. Acad. Sci. U. S. A.* **2015**, *112*, 12486−12491.
(39) Guo, S.; Nakagawa, Y.; Barhoumi, A.; Wang, W.; Zhan, C.; Tong, R.; Santamaria, C.; Kohane, D. S. *J. Am. Chem. Soc.* **2016**, *138*, 6127−6130.
(40) Kearney, C. J.; Mooney, D. J. *Nat. Mater.* **2013**, *12*, 1004−1017.
(41) Hsu, B. B.; Park, M.-H.; Hagerman, S. R.; Hammond, P. T. *Proc. Natl. Acad. Sci. U. S. A.* **2014**, *111*, 12175−12180.
(42) Yang, S. C.; Bhide, M.; Crispe, I. N.; Pierce, R. H.; Murthy, N. *Bioconjugate Chem.* **2008**, *19*, 1164−1169.
(43) Palamoor, M.; Jablonski, M. M. *Mol. Pharmaceutics* **2013**, *10*, 701−708.
(44) Ryu, J. H.; Chacko, R.; Jiwpanich, S.; Bickerton, S.; Babu, R. P.; Thayumanavan, S. *J. Am. Chem. Soc.* **2010**, *132*, 17227−17235.
(45) Zhuang, J.; Jiwpanich, S.; Deepak, V. D.; Thayumanavan, S. *ACS Macro Lett.* **2012**, *1*, 175−179.
(46) Hansch, C.; Leo, A.; Taft, R. W. *Chem. Rev.* **1991**, *91*, 165−195.
(47) Jiwpanich, S.; Ryu, J. H.; Bickerton, S.; Thayumanavan, S. *J. Am. Chem. Soc.* **2010**, *132*, 10683−10685.
(48) Okamoto, Y.; Inukai, T.; Brown, H. C. *J. Am. Chem. Soc.* **1958**, *80*, 4972−4976.
(49) Knipe, J. M.; Peppas, N. A. *Regen. Biomater.* **2014**, *1*, 57−65.
(50) Lee, K.; Rafi, M.; Wang, X. J.; Aran, K.; Feng, X. L.; Lo Sterzo, C.; Tang, R.; Lingampalli, N.; Kim, H. J.; Murthy, N. *Nat. Mater.* **2015**, *14*, 701−706.
(51) Murthy, N.; Xu, M.; Schuck, S.; Kunisawa, J.; Shastri, N.; Fréchet, J. M. J. *Proc. Natl. Acad. Sci. U. S. A.* **2003**, *100*, 4995−5000.
(52) Sy, J.; Seshadri, G.; Yang, S.; Brown, M.; Oh, T.; Dikalov, S.; Murthy, N.; Davis, M. E. *Nat. Mater.* **2008**, *7*, 863−868.

DOI: 10.1021/jacs.6b11181
J. Am. Chem. Soc. 2017, 139, 2306−2317